Pyridine on Colloidal Silver. Polarization of Surface Studied by Surface-Enhanced Raman Scattering and Density Functional Theory Methods

ARTICLE *in* THE JOURNAL OF PHYSICAL CHEMISTRY C · FEBRUARY 2010

Impact Factor: 4.77 · DOI: 10.1021/jp912071a

3 AUTHORS:

A. Kaczor
Jagiellonian University
64 PUBLICATIONS **540** CITATIONS
SEE PROFILE

Kamilla Malek
Jagiellonian University
47 PUBLICATIONS **224** CITATIONS
SEE PROFILE

Malgorzata Baranska
Jagiellonian University
159 PUBLICATIONS **1,859** CITATIONS
SEE PROFILE

Pyridine on Colloidal Silver. Polarization of Surface Studied by Surface-Enhanced Raman Scattering and Density Functional Theory Methods

Agnieszka Kaczor,* Kamilla Malek, and Malgorzata Baranska

Faculty of Chemistry, Jagiellonian University, Ingardena 3, 30-060 Krakow, Poland

Received: December 22, 2009; Revised Manuscript Received: February 2, 2010

Surface-enhanced Raman scattering (SERS) spectra of pyridine in various Ag colloids with different excitation wavelengths (514.5 and 1064 nm) were recorded and compared with the theoretical models computed with application of the static density functional theory method in order to simulate the chemical enhancement. Pyridine was chosen as a model compound to look at the surface enhancement since it is a well-known and extensively studied molecule by using SERS spectroscopy, and hence of great significance to the subject. Moreover, it was the first species for which a SERS spectrum obtained on electrochemically roughened silver surface was reported. The arrangement of pyridine on metal particles in the solution allows neglecting the solvent effects and placing the focus only on the interaction between adsorbent and metal surface to study the SERS mechanism. The intensity of bands in the fingerprint region of pyridine SERS spectra depends not only on the excitation wavelength but also on the applied colloid and the way in which it is activated or the potential of the electrode if such methodology is applied. With the help of theoretical calculations using various models of pyridine in the presence of silver nanoparticles, several parameters are predicted (e.g., the charge of the pyridine nitrogen, $N-Ag_{adatom}$ distance). Good reproducibility of relative intensities of the Raman bands in the SERS spectra was achieved with the application of theoretical models and related to the polarization of the metal surface. The polarization of the surface, experimentally induced by increase of the negative potential of the electrode or adding chloride ion to the colloid, was reproduced computationally by varying of the size of cluster models (using systems with 5, 9, and 25 Ag atoms) and including chloride ions in the computed models (with negative charge set on Cl in the nine-silver-atom model).

Introduction

Pyridine (pyr) was the first species for which a surface-enhanced Raman scattering (SERS) spectrum, obtained on electrochemically roughened silver surface, was reported.[1] The origin of the enhancement was, however, not properly recognized up to 1977, when Albrecht and Creighton[2] and Jeanmaire and Van Duyne[3] indicated two effects, charge-transfer and electromagnetic, as being responsible for the observed anomalously intense Raman signal of pyridine adsorbed on a silver electrode. Up to now, the chemical (CE, involved with charge transfer between the adsorbed molecule and the surface together with changes in the electronic structure of the molecule upon adsorption) and electromagnetic (EM, due to excitation of plasmon oscillations) mechanisms are widely accepted as major mechanisms by which enhancement of adsorbed substrates is accomplished. For pyridine, both mechanisms have been proven to contribute to the enhancement,[3−6] resulting in an increase of the intensity of several bands whose frequencies strongly depend on the type of SERS active system. For pyridine adsorbed on a roughened electrode, frequencies of the bands are quite conserved, and a set of features at ca. 624, 1010, 1035, 1218, and 1598 (±7) cm^{-1} is observed.[1,2,5,7,8] Nevertheless, the changes in potential at the electrode produced changes in the relative intensity of these bands and the appearance of new signals, particularly at 1025 cm^{-1}, assigned to pyridine coordinated to silver.[1] The SERS spectra of pyridine absorbed on silver colloids vary strongly with experimental conditions of colloid composition, preparation, and aging.[9−12] Particularly, SERS spectra of pyridine in the presence of halides in a silver hydrosol differ markedly with respect to spectra obtained in halide-free colloids.[9,10,12−14] In general, the spectra of pyridine obtained on colloids are richer than spectra recorded on electrodes, particularly for colloids containing chloride ions.[9,10,12] It was suggested that the presence of Cl^- intensifies the charge-transfer effect allowing formation of coordinate-like compounds of a pyr-$(Ag_n)^{y+}$ type ($n = 2, 3, 4$; $y = 1, 2$), based on density functional theory (DFT) computations.[9,10,12,13] These and several other small (up to five silver atoms), both charged and neutral, clusters were considered at DFT and ab initio calculations as models for the SERS effect.[6,9−13,15−19] Most of these works considered chemical enhancement only and predicted the CE factor to be not more than 10,[9−13,15,17−19] although Wu et al.[6] obtained as much as 93 times increase in Raman scattering factor for a ring symmetric stretching mode υ_{8a} for the $Py-Ag_4$ system.

In general, understanding of chemical enhancement and proving it experimentally is difficult, as the effect is quite badly defined and, additionally, difficult to separate from the electromagnetic enhancement. The chemical enhancement is significantly bigger in the case of resonance of excitation wavelength with a molecular transition or cluster−adsorbate CT transition. The CE factor was experimentally estimated from 30 for pyrromellitic dianhydride on copper[20] up to 10^6 for SERRS CE factor for rhodamine 6G.[21] For pyridine, CE enhancement was estimated as 15−65 by Jing and Campion[22] based on the spectrum obtained on Rh(100) with a thickness of 10% of a silver monolayer. Obviously, the CE effect is more prominent for molecules that can be chemisorbed on the surface of metal, as pyridine, and works on short distance only (up to 20 Å).[23]

* Corresponding author. E-mail: kaczor@chemia.uj.edu.pl.

10.1021/jp912071a
Published on Web 02/17/2010

Nevertheless, it is widely accepted that CE is "covered" by electromagnetic mechanism, which produces a stronger enhancement.

Recently, Schatz et al.[4,24] presented TDDFT calculations of the SERS spectrum of pyridine based on a pyridine−Ag_{20} cluster, comparing it also with the calculations for smaller pyridine−Ag models (n = 2, 4, 6, 8). These calculations indicated that a 20-atom silver cluster is a reliable model of larger nanoparticles and allowed for prediction of the enhancement factors for the pyridine−Ag system, with static chemical enhancement factor (associated with the change of electron density due to the presence of metal) estimated to be ca. 10 compared with 10^3 and 10^5 suggested for enhancement due to charge-transfer and electromagnetic mechanism, respectively.[4,24] As one can notice, the electromagnetic enhancement is predicted to influence Raman intensity and is indeed bigger compared to the chemical enhancement. Nevertheless, due to surface selection rules, vibrations transforming as the same irreducible representation shall be enhanced in a similar way due to the electromagnetic effect.[25,26] Therefore, it is the chemical enhancement that shall considerably differentiate Raman intensities of the modes belonging to a given representation.

We obtained SERS enhanced spectra of pyridine on different Ag colloids with different exciting wavelengths and compared them with the theoretical models computed with the application of the static DFT method in order to reproduce chemical enhancement. Pyridine was chosen, as it is an ideal model compound to study surface enhancement, due to the broad literature about the subject, and therefore known arrangement of pyridine on silver surface and minimization of the solvent effects (it is assumed that "bonding" of the polar nitrogen atom of the chemisorbed pyridine with the silver adatom leaves only a nonpolar ring to interact with the solvent). Spectra based on different computed models are compared with pyridine SERS spectra obtained in various silver colloids and different excitation wavelengths (514.5 and 1064 nm) and the SERS pyridine spectra obtained on electrode (514.5 nm).[14] The polarization of the surface, experimentally induced by increase of the negative potential of the electrode or adding chloride ion to the colloid, was successfully reproduced computationally by varying the size of metal cluster models and including chloride ions in the computed models.

Materials and Methods

Experimental Section. For Fourier transform−near infrared (FT−NIR) Raman measurements, the liquid pyridine and its aqueous solution (pyridine:H_2O = 1:1) were measured in glass capillaries. One thousand twenty-four scans were collected (with a resolution of 4 cm^{-1}) with the output power of the laser of 800 mW for both samples. Spectra were recorded on the FT−Raman Spectrometer Nicolet NXR 9650 equipped with a Nd:YAG laser, emitting at 1064 nm, and a germanium detector cooled with liquid nitrogen. Additionally, the Raman spectra of the pyridine samples were measured with a Renishaw Confocal Raman Microscope System (model *inVia*) equipped with the Ar^+ laser (514.5 nm), a Leica DMDL microscope, and CCD camera, working under microconditions with an objective 5×. Twenty-four and eight scans, for sole pyridine and its aqueous solution, respectively, were collected with a resolution of 2 cm^{-1}. The output laser power was 10 mW.

The hydroxylamine HCl was used to prepare the silver colloid (hereafter Ag−CDX) following the procedure of Leopold and Lendl.[27] Also, silver colloids were prepared following Creighton's procedure[28] by adding silver nitrate to an aqueous solution of excess sodium borohydride as a reducing agent (hereafter Ag−BH_4) and by reduction with citrate according to the method of Lee and Meisel (hearafter Ag−citrate).[29] The sample of pyridine for the SERS measurements was prepared in aqueous solutions with concentration of 1×10^{-3} mol·dm^{-1}. The final concentration in SERS was 2 orders of magnitude lower than initial concentrations. All the reagents employed were of analytical grade and were prepared using fourfold distilled water. The colloids were activated before addition of pyridine by using potassium nitrate or potassium chloride. To accomplish this, 20 μL of 0.5 mol·dm^{-1} solution of the activator was added to 0.5 mL of the colloid, and then 5 μL of the sample was added. The SERS spectra with the excitation lines at 1064 and 514.5 nm were recorded with the instruments described above. The output laser powers were set at 500 and 10 mW, respectively, while 1024 and 8 scans were recorded for NIR and vis excitation lines, respectively.

For the recording of the absorption spectra of the aqueous solution of pyridine with a concentration of 1×10^{-5} mol·dm^{-1} and silver colloids, a UV−vis spectrophotometer, model HP 8452, was used with a resolution of 2 nm in a range of 190−820 nm. Quartz cells of 1 cm were used. Absorption bands were observed at the following wavelengths: for pyridine − λ_{max} = 266 nm; for colloids, Ag−CDX − λ_{max} = 412 nm; Ag−BH_4 − λ_{max} = 394 nm, Ag−citrate − λ_{max} = 420 nm; and for pyridine on the activated silver colloids, $\lambda_{max}^{Ag-CDX,KNO3}$ = 408 nm, $\lambda_{max}^{Ag-CDX,KCl}$ = 410 nm, $\lambda_{max}^{Ag-BH4,KNO3/KCl}$ = 394 nm, and $\lambda_{max}^{Ag-citrate,KNO3}$ = 420 nm.

Computational Methodology. The quantum chemical calculations were performed with Gaussian03,[30] using a DFT method to optimize geometry and compute vibrational wavenumbers, infrared intensities, and Raman activities of pyridine and pyridine−metal clusters. The DFT calculations were carried out with the three-parameter density functional abbreviated as B3LYP, which includes Becke's gradient exchange correction[31] and the Lee, Yang, and Parr correlation functional.[32] The DGDZVP basis set, of a size of a polarized double-ζ basis set,[33] was applied in calculations involving silver and water. For the computations regarding sole pyridine, the LANL2DZ, 6-311++G(d,p), and cc-pV5Z basis sets were additionally used. For clusters, geometrical parameters were optimized using the geometry direct inversion of the invariant subspace (GDIIS) method.[34,35] The cPCM polarizable conductor calculation model[36,37] was applied for the pyridine−water complex. The GAPT (generalized atomic polar tensor) population analysis[38] was applied to calculate the atomic charges of the molecule. The charge of an atom is defined as 1/3 of the sum of the first dipole moment derivatives with respect to its Cartesian coordinates.

The obtained Raman activities were recalculated for Raman intensities using the RAINT[39] program. The B3LYP/6-311++G(d,p), B3LYP/DGDZVP, and B3LYP/cc-pV5Z calculated harmonic frequencies were scaled down by a factor of 0.980, 0.985, and 0.980, respectively, to account mainly for anharmonicity effects and limitations of the basis set. Potential energy distributions (PED) of the normal modes of pyridine were computed in terms of natural internal coordinates[40] with the GAR2PED[41] program.

Results and Discussion

Structure of Pyridine and the Pyridine−Ag_{25}. The optimized (B3LYP/DGDZVP) geometry of pyridine and pyridine−Ag_{25} cluster is presented in Figure 1 along with calculated GAPT charges.

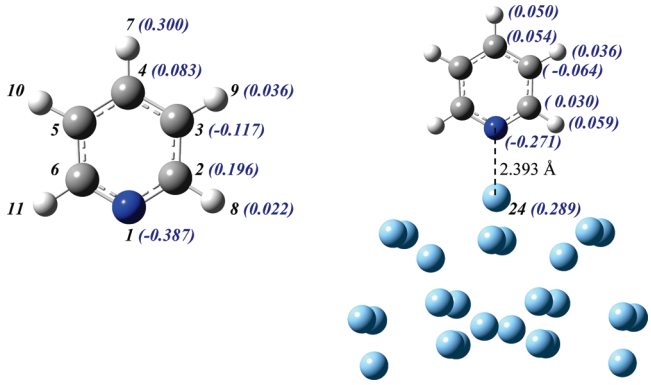

Figure 1. Optimized (B3LYP/DGDZVP) geometry of pyridine and pyridine−Ag_{25} cluster with the atom numbering scheme (in italics) and GAPT charges (in au, in parentheses in blue).

Five small imaginary frequencies have been found for the cluster, but as their magnitude is very small (less than 16 cm^{-1}) the structure can be treated as a minimum. The C_{2v} symmetry of pyridine was also preserved in the pyridine−Ag_{25} model. The input structure of the cluster was constructed with the 25 silver atoms set in one layer and the pyridine molecule placed perpendicularly to the surface of a metal. The optimization significantly perturbed this structure resulting in a quasi-tetrahedral arrangement of silver atoms and formation of an adatom at the distance of 2.393 Å to the pyridine nitrogen atom. Although the geometrical parameters predicted by computations for a pyridine in the model are very similar to the parameters obtained for a pyridine itself (Table S1, Supporting Information), the charge distribution changed considerably. Calculated GAPT charges, presented in Figure 1, indicate the shift of the electron density producing the overall negative charge of pyridine (−0.045 au) in the complex. Depolarization of the N−C bonds and polarization of the silver adatom, which, according to the calculations, gains substantial positive charge (0.298 au), is predicted. The small distance (2.393 Å) between the nitrogen atom and the silver adatom, along with polarization of the latter, suggests the chemisorption of pyridine on the surface of silver.

Additionally, energetic effects of bending of the pyridine molecule toward the plane of the cluster and turning it along the $Ag_{ad}-N_1-C_4-H_7$ line have been estimated based on potential energy scans along relevant coordinates (see Figure 2).

The model cluster applied in these scans was minimized to nine silver atoms. As expected, calculations predict that bending of the plane of the molecule toward the plane of metal increases the energy of the system. For example, for $H_8-C_2-N_1-Ag_{ad}$ equal to 90°, with the pyridine ring hovering above the metal plane, the energy is estimated as ca. 28 kJ mol^{-1} over the input structure, where the plane of the ring is exactly perpendicular to the surface of metal. Nevertheless, the small deviation from perpendicularity does not increase energy significantly, i.e., structures with $H_8-C_2-N_1-Ag_{ad}$ equal to 5, 10, or 15° are destabilized energetically less than 1 kJ mol^{-1} compared to the fully perpendicular arrangement. Turning the molecule around the N_1-Ag_{ad} line produces practically no effect on the energy of the pyridine−Ag_9 model. Both these results demonstrate that the molecule has considerable freedom of movement with respect to the plane of the cluster and that there are many arrangements of the pyr molecule over the cluster possible unless the plane of the molecule is *significantly* bent over the plane of the metal (these arrangements are energetically disfavored).

The binding energy of pyridine chemisorbed to silver adatom has been roughly estimated as 32 kJ mol^{-1} when investigating

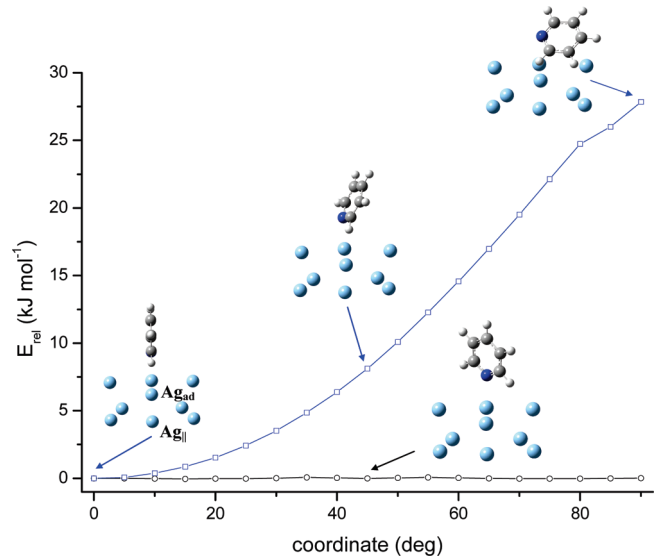

Figure 2. Potential energy scans (B3LYP/DGDZVP) of the pyr−Ag_9 cluster along the $H_8-C_2-N_1-Ag_{ad}$ angle (bending of the pyr molecule over the surface of the metal; blue line) and $C_2-N_1-Ag_{ad}-Ag_{||}$ (rotation around N−Ag bond; black line). For numbering scheme, refer to Figure 1.

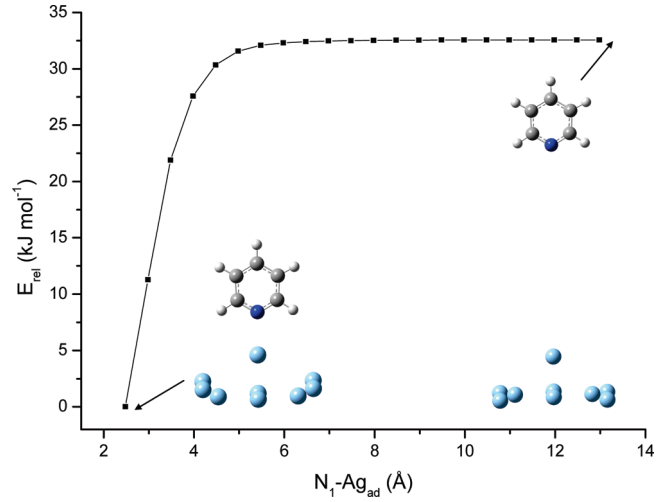

Figure 3. Potential energy scan (B3LYP/DGDZVP) of the pyr−Ag_9 cluster along the N_1-Ag_{ad} distance. For the numbering scheme, refer to Figure 1.

the energy changes associated with the increase of the distance between the nitrogen pyridine atom and the silver adatom (see Figure 3). The energy of the cluster is predicted to increase steeply with the increase of the N_1-Ag_{ad} distance, achieving a plateau at the distance of ca. 6 Å, from which the change of energy is practically negligible (the energy difference between structures with the distance ca. 13 Å and ca. 6 Å is 0.27 kJ mol^{-1}.)

Raman Spectra of Pyridine. Figure 4 presents Raman spectra of pyridine and pyridine−water 1:1 solution obtained with 514.5 and 1064 nm excitation wavelengths compared with the theoretical Raman spectra of pyridine (B3LYP/DGDZVP and B3LYP/cc-pV5Z). This comparison was done in order to (1) check the reliability of the data obtained at the B3LYP/DGDZVP level of theory, applied later to simulation of the SERS spectra, and (2) recognize the influence of the water environment on the Raman shifts of pyridine as the SERS spectra of pyridine were registered in aqueous solutions. The detailed list of frequencies and Raman intensities of pyridine

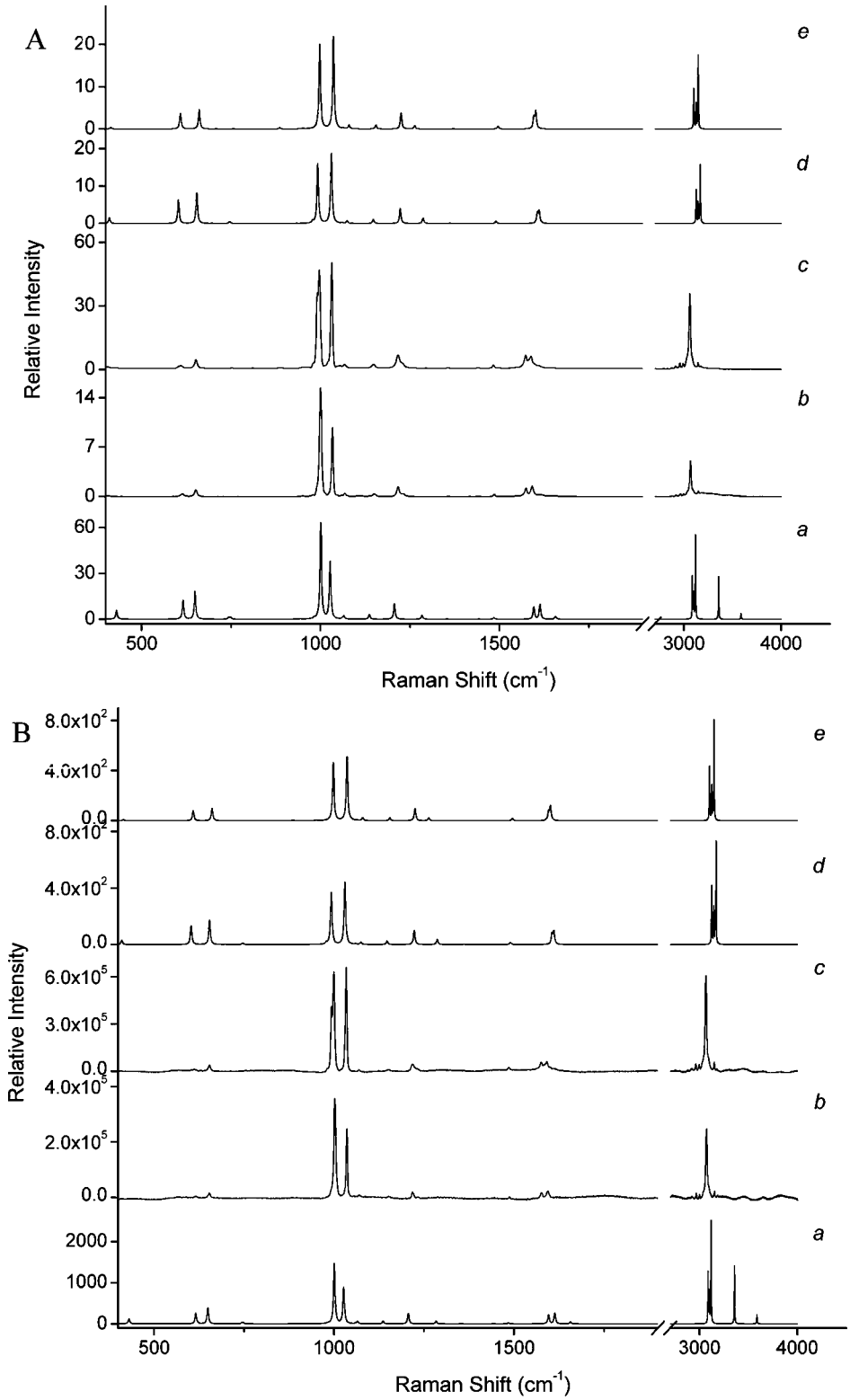

Figure 4. Raman spectra of aqueous solution of pyridine 1:1 (b), pyridine (c), theoretical spectra of pyridine obtained at the B3LYP/DGDZVP (d) and B3LYP/cc-pV5Z (e) levels of theory, and the theoretical spectrum of pyridine−water complex [(a) cPCM, B3LYP/DGDZVP]; excitation with 1064 nm (A) and 514 nm (B) light. Theoretical spectra have been broaden by a Lorentzian having a width of 5 cm^{-1}.

calculated with the application of four different basis sets is given in Table S2 of the Supporting Information.

B3LYP/LANL2DZ, the level of theory commonly applied to computations of pyridine−Ag clusters, does not reproduce experimental spectra correctly (see Table S2). The most intense bands in the fingerprint regions, observed at 996 and 1031 cm^{-1} for 1064 nm excitation, are predicted at 989 and 1042 cm^{-1} at the B3LYP/LANL2DZ level (no scaling), with the separation between these signals of 53 cm^{-1} that cannot be corrected significantly by application of a scaling factor. In the case of other methods, the predicted separation of the Raman shifts of these bands is in the range of 36−40 cm^{-1} and agrees well with the experimentally observed difference of 35 cm^{-1}. Moreover, the Raman shifts obtained at the B3LYP/LANL2DZ level differ

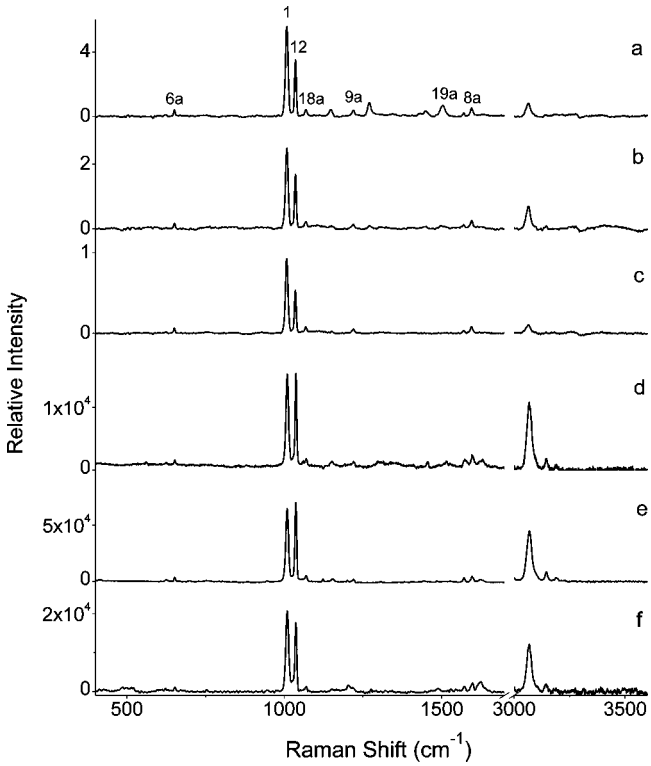

Figure 5. SERS spectra of pyridine obtained on the Ag−CDX colloid activated with KCl (a, 1064 nm; d, 514 nm) and KNO_3 (b, 1064 nm; e, 514 nm), Ag−citrate (activated with KCl; c, 1064 nm) and Ag−BH_4 (activated with KCl; f, 514 nm).

considerably with the experimental ones, in the sense not only of frequencies but also of relative intensities. All other applied basis sets (DGDZVP, 6-311++G(d,p), and cc-pV5Z), although of different quality (2ζ, 3ζ, and 5ζ, respectively), very reasonably reproduced the experimental data. In particular, the results obtained with the application of the 5ζ-quality and 2ζ-quality basis sets are very similar (see Figure 4) with the relative error being for the latter not more than 2% in the fingerprint range showing that the B3LYP/DGDZVP level is fully adequate to simulate Raman spectra of pyridine.

The Raman shifts of pyridine in the aqueous solution differ from the Raman shifts of pure pyridine up to 4 cm^{-1} in the fingerprint region (see Figure 4 and Table S4 of the Supporting Information, λ_{514nm} and λ_{1064nm}). The direction of changes depends on the band (both red and blue shifts are observed in the spectrum of water solution of pyridine compared to pure pyridine) and are coincident with the direction of changes of frequencies in the pyr SERS spectra (please refer to the next section). It is necessary to emphasize that the shift of the bands in the aqueous solution is quite small compared to the shift of the bands taking place in the silver colloid, showing that changes of the electron density upon solvation are quite subtle. Molecular dynamic simulations of solvation dynamics of pyridine in water showed that the pyridine is H-bonded to one solvent molecule.[12] Therefore, the cPCM polarizable conductor calculation model[36,37] was used to optimize geometry and predict normal frequencies of the 1:1 model of the pyridine:water complex at the B3LYP/DGDZVP level. Indeed, the observed shift is nicely reproduced in the theoretical spectra (see Figure 4 and Table S4 of the Supporting Information).

SERS Spectra of Pyridine versus the Computational Model Spectra. The SERS spectra of pyridine in silver colloids are presented in Figure 5. Figure 6 shows Raman spectra of the

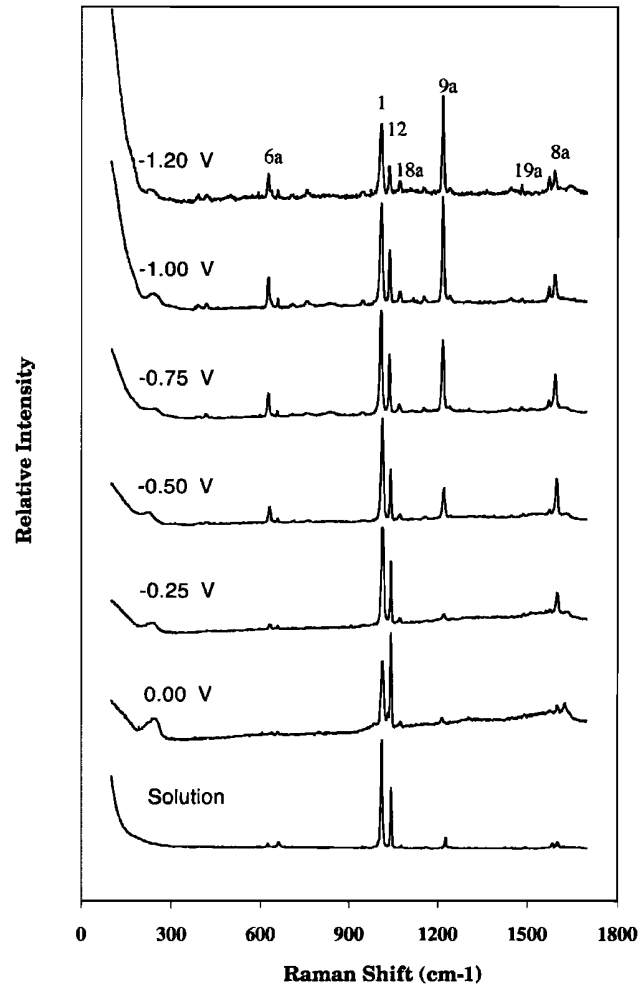

Figure 6. Raman pyridine spectra of the aqueous solution and SERS of pyridine on silver electrode (excitation with 514 nm, from ref 14 obtained with the permission of the American Chemical Society).

aqueous solution of pyridine and SERS of pyridine on silver electrode obtained by Arenas et al.[14] with the excitation wavelength of 514 nm. The simulated spectra of chosen pyridine−Ag clusters (B3LYP/DGDZVP) for the 1064 nm excitation wavelength are presented in Figure 7 (the computed spectra with 514 nm excitation are practically the same in the fingerprint region; therefore, they are not shown). Raman shifts of pyridine obtained on different colloids and using both excitation wavelengths are summarized in Table S5 of the Supporting Information and compared to theoretical results for the model clusters. The computations were applied to reproduce the observed Raman shifts and additionally, as all vibrations transforming as the same irreducible representation shall be enhanced similarly due to the electromagnetic effect, the computationally predicted Raman intensities of the bands belonging to a given representation shall approximately model the relative SERS intensities.

As it was mentioned above, the directions of changes in the SERS spectra are like changes occurring upon hydratation of pyr (apart from one band at 1573 cm^{-1} in the pure pyridine spectrum). For example, two very intense bands at 996 and 1031 cm^{-1} in the pyridine spectrum (assigned to the υ_1 and υ_{12} mode, respectively) are placed at 1000 and 1033 cm^{-1} in the aqueous solution of pyridine spectrum (1:1) and at 1008 and 1036 cm^{-1} in the SERS spectra of pyridine on Ag colloids (λ_{1064nm}). This indicates that the redistribution of electron density of pyridine upon H-bond formation or chemisorption on the Ag adatom is

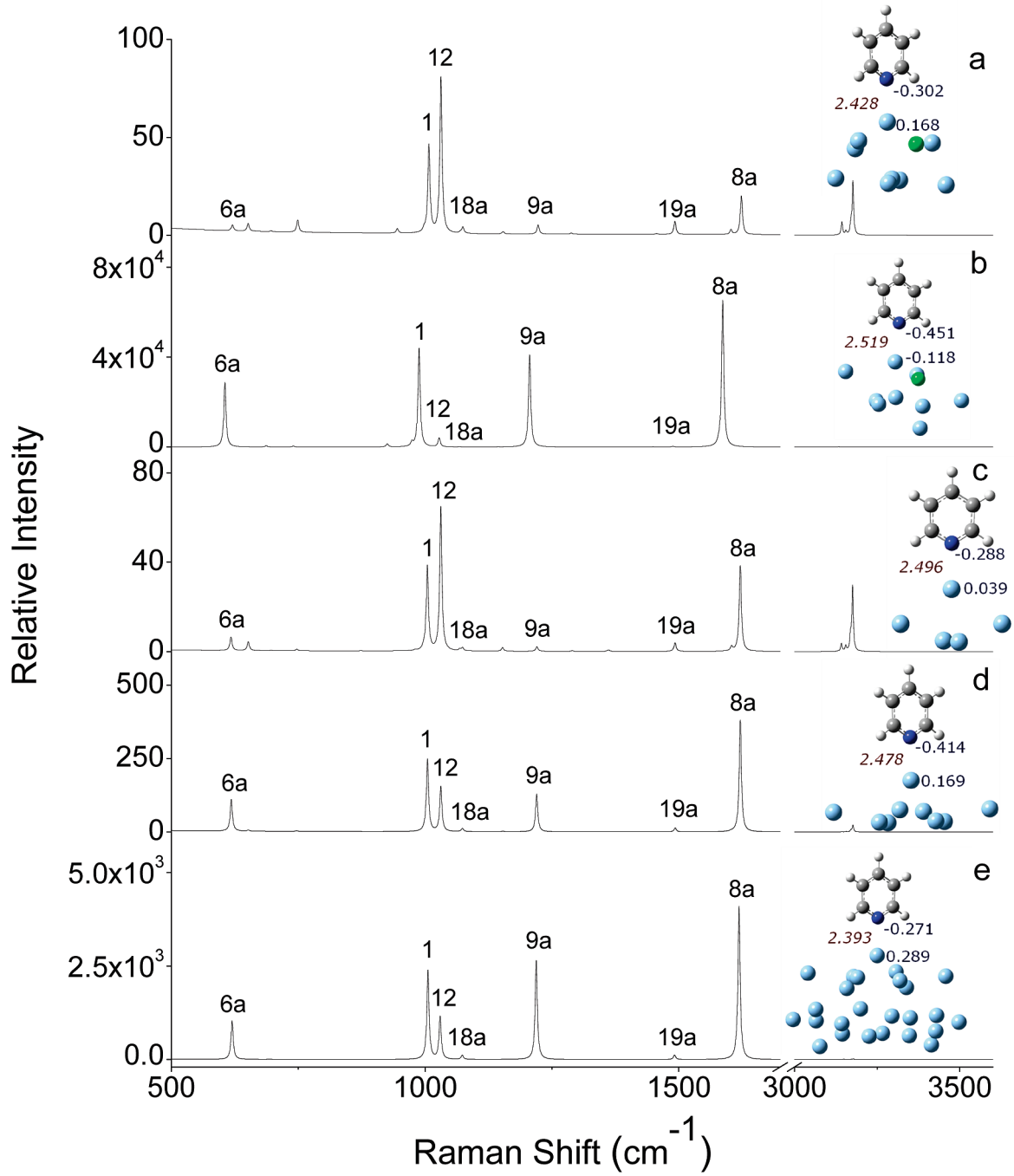

Figure 7. Calculated Raman spectra of pyr−Ag models: pyr−Ag_9−Cl (a), pyr−Ag_9−Cl^- (b), pyr−Ag_5 (c), pyr−Ag_9 (d), pyr−Ag_{25} (e), excitation with 1064 nm. Theoretical spectra have been broaden by a Lorentzian having a width of 5 cm^{-1}. Numbers in brown denote a distance between the nitrogen atom and the silver adatom (in Å), and numbers in blue show the atomic charges (predicted GAPT charge for the nitrogen in sole pyr is −0.387 au).

quite similar, which is not so unusual taking into account that the nitrogen atom is affected mainly in both these cases.

Additionally, experimental spectra obtained with the excitation wavelength of 514 and 1064 nm differ significantly, in the sense of both Raman shift values and intensities of the bands. Differences are also observed in the case of spectra obtained at different colloids and also in the case when the same colloid is activated with different salts. The most intense bands in the fingerprint region of the SERS spectra of pyridine at Ag colloids are observed at 1010/1037 and 1008/1036 cm^{-1} (υ_1/υ_{12} according to the Wilson notation, which is going to be used throughout this text) for the excitation of 514 and 1064 nm, respectively. There is a striking change of the ratio of intensity of these bands observed in case of spectra obtained with both excitation wavelengths. The intensity ratio of the 1008 cm^{-1} (υ_1) to 1036 cm^{-1} (υ_{12}) band in the SERS spectra excited with the 1064 nm line is over 2:1, while for the same bands with 514 nm excitation this ratio is not more than 1.2−1.8:1.

In general, the υ_1/υ_{12} ratio depends on the excitation wavelength, but also on the applied colloid and the way in which it is activated. For 514 nm excitation the υ_1/υ_{12} ratio was ca. 1.5, 1.3, and 1.7 for Ag−CDX with KCl, Ag−CDX with KNO_3, and Ag−BH_4 with KCl, respectively. For NIR excitation, the ratio was ca. 2.4, 2.2, and 2.6 for Ag−CDX with KCl, Ag−CDX with KNO_3, and Ag−citrate with KCl, respectively.

It was previously demonstrated that the υ_1/υ_{12} ratio is sensitive to the presence of Cl^- ions in silver hydrosols with the intensity of the υ_1 band increasing systematically with respect to υ_{12} with the growth of the concentration of chloride ions.[9,28] Analogical changes of intensity of the υ_1 versus υ_{12} band were noticed for SERS spectra of pyridine on silver with the increase of the negative potential of the electrode (see Figure 6).[14,42] In both cases the variation of surface charge is achieved, resulting in increase of intensity of some individual bands, namely, the υ_{6a}, υ_{8a}, υ_{9a}, and already mentioned υ_1 band. This effect was clearly observed in the case of the SERS spectra on the Ag−CDX colloid in the presence of Cl^- ions. For spectra of pyridine on CDX colloid, the υ_1/υ_{12} ratio in the presence of Cl^- ions was ca. 0.2 times higher than in the absence of the halide ions, and the effect was clearly independent of the excitation wavelength.

Very interesting differences are observed when spectra of different colloids are compared. The NIR−SERS spectra of pyridine obtained on the Ag−CDX colloid activated with halide ions (see Figure 5a) are markedly altered relative to all other SERS spectra, i.e., those obtained at different colloids, with different excitation wavelength, or in the absence of Cl^- ions. This spectrum is quite repeatable; it was obtained two times for three different colloid preparations. The striking feature of this spectrum is a significant increase of the intensity of the bands at 1505, 1450, 1270, and 1149 cm^{-1}, assigned to υ_{19a}, υ_{19b}, υ_{15}, and υ_3 modes, respectively. Comparison of NIR−SERS spectra obtained on the Ag−CDX colloid, but activated with NO_3^- ions (see Figure 5b), demonstrates that these bands are also present, although their intensity is very weak. Nevertheless, they were not observed when other colloids were applied (see Figure 5c and Table S5). It is the common truth that the SERS spectra obtained on different colloids differ significantly as their morphology and aggregation differ. The very approximate size of particles of silver colloids obtained according to the methods of Creighton et al.,[28] Leopold and Lendl,[27] and Lee and Meisel[29] is 10, 50, and 100 nm, respectively, although it varies in a very broad range depending on the exact preparation procedure (for example, the hydroxylamine colloid size might be in the range of 23−67 nm depending on mixing order and rate[27]). Additionally, activation of colloids by anions may produce aggregation and/or diffusion of aggregates formed[43] that significantly changes the morphology of the particles. In general, citrate was indicated as the more suitable for use with NIR excitation as its aggregation process produces a wide range of aggregates.[43] Indeed, we obtained SERS spectra on a citrate colloid activated with KCl for both 514 and 1064 nm excitation, while recording of the NIR excited SERS spectra on borohydride was not possible. For the latter colloid, the UV/vis spectra indicated considerable decrease of absorption while going toward longer wavelengths. Similar decrease of absorbance toward longer wavelengths was also detected for citrate activated with KNO_3, for which NIR SERS spectra were indeed of very low intensity compared with the spectrum of the citrate colloid activated with KCl. In our case, the biggest enhancement was obtained for SERS spectra obtained on the silver colloid prepared by reduction with hydroxylamine. Cañamares et al.[44] demonstrated that the hydroxylamine colloid exhibits high SERS effectiveness and large adsorption surface compared to colloidal particles obtained by chemical reduction by citrate, laser ablation, and laser in situ photoreduction. Our results are in agreement with this conclusion.

As a next step, we decided to compare obtained experimental results with the computational models (see Figure 7). There were two "types" of models that have been optimized: the extended, built out of 25 atoms of silver (pyridine−Ag_{25}), and the contracted with only 9 and 5 atoms of silver (pyridine−Ag_9 and pyridine−Ag_5, respectively). The 5 and 25 silver atoms were chosen for the models as two limiting cases: the first as the smallest cluster for which changes in the proper direction in the relative intensities of the bands are noticed compared to the Raman spectrum of pyr, and the latter as a "big model" case, but still computationally feasible in our conditions. The 9-atom cluster was built as "an intermediate case" and can treated as "a derivative" of a 25-atom model in which most distant "layers" of metal were removed and only 3 layers of metal atoms can interact with pyridine. In this way it allowed comparing directly the relation between the number of metal atoms, the N−Ag_{ad} distance, and polarization of the metal surface. Additionally, the possible changes of the metal surface charge have been considered by optimizing clusters with the positive charge added to pyridine−Ag_{25} (pyridine−Ag_{25}^+) or a positive charge and a chloride ion (pyridine−Ag_9−Cl) or a sole chloride ion (pyridine−Ag_9−Cl^-) added to the pyridine−Ag_9 model. Although calculations of vibrational frequencies of optimized geometries of all described models resulted in imaginary frequencies assigned to the silver lattice vibrations or the vibration of the whole pyridine molecule with respect to the silver cluster, their values were very small (not bigger than ca. 15 cm^{-1}) for all computed clusters apart from $(pyridine-Ag_{25})^+$ (for which the lowest frequency is ca. 54 cm^{-1}). Therefore, all clusters apart from the latter are considered to be practically minima on their potential energy surfaces. The charged $(pyridine-Ag_{25})^+$ model, which resulted after frequency calculations in a negative frequency of ca. 54 cm^{-1}, did not reproduce the experimental SERS spectra (see Figure S1, Supporting Information), and hence it was excluded from further discussion.

Apparently, the relative intensities and vibrational frequencies for these models differ considerably. Four of the models, namely, pyridine−Ag_{25}, pyridine−Ag_9, pyridine−Ag_5, and pyridine−Ag_9−Cl, resulted in the predicted vibrational frequencies being in excellent agreement with the experimental Raman shifts in SERS spectra of pyridine (the relative error is not more than 2.2% and the average one not more than 0.8% in the fingerprint region). The pyridine−Ag_9−Cl^- model reproduces obtained Raman shifts just a bit worse compared to four above-mentioned clusters (the maximum relative error in the fingerprint range is ca. 3%, while the average one is 0.9%, respectively). Therefore, based on the sole comparison of frequencies, the evaluation of the models is practically impossible. Very interesting conclusions, however, might be drawn from the comparison of relative intensities of computed models.

The increase of the number of silver atoms (see Figure 7c, d, and e) resulted in a dramatic change of intensities of SERS bands. These changes in the theoretical spectra can be very well correlated with the changes of SERS spectra of pyridine absorbed on silver electrode under increase of its negative potential (see Figure 6[14,42]). At the potential of 0 V, there are two bands of pyridine significantly enhanced in the SERS spectrum: υ_1 and υ_{12} with the intensity ratio of υ_{12}/υ_1 being over 1 (see Figure 6[14,42]). This might be strictly related with the pyr−Ag_5 model spectrum, apart from the fact that the υ_{8a} band is overestimated in the latter (in fact, it is overestimated in all models). The increase of potential of the electrode results in the relative increase of several a_1 symmetry bands, mainly, υ_{6a}, υ_1, υ_9, and υ_{8a} (see Figure 6[14,42]). This behavior is very well reproduced by our cluster models in which the same changes are predicted upon increase of the number of silver

atoms. This increase of silver atoms in the model resulting in the above-mentioned changes of the relative intensities of bands can be correlated with the optimized $N-Ag_{adatom}$ distance in the models (2.497, 2.478, and 2.393 Å for models with 5, 9, and 25 Ag atoms, respectively) and the SERS enhancement (the band-dependent 2−10-fold increase between the pyridine$-Ag_5$ and pyridine$-Ag_9$ model is noticed with ca. 10-fold increase between pyridine$-Ag_9$ and pyridine$-Ag_{25}$ model). Additionally, the GAPT charge on the adatom is the factor that is related to the size of the cluster (0.039, 0.169, and 0.289 for pyr$-Ag_5$, pyr$-Ag_9$, and pyr$-Ag_{25}$). The GAPT charge of the adatom represents the polarization of the surface and undoubtedly shows that its increase produces enhancement of intensity of a_1 symmetry bands (particularly υ_{6a}, υ_1, υ_9, and υ_{8a}). It might be concluded that increase of the number of silver atoms in a model allows reproduction of relative intensities of the bands as the number of metal atoms reflects the polarization of the metal surface. This polarization of the surface might be much easier observed on the electrode upon increase of its potential (see Figure 6), while the effects of introduction of chloride ions observed on colloidal silver are much more subtle (compare the υ_1/υ_{12} ratio in Figure 5a versus b and d versus e). In fact, the surface of the electrode is much easier to model due to the fact that it is more ordered and rigid. The aggregation of colloid produced nonrigid and punctually chaotic surface that results in enhancement of non-a_1 symmetry modes (discussed above, see Figure 5a). The activation of colloid by halides was modeled by adding of a chloride atom (see Figure 7a) or ion (see Figure 7b) to the nine-silver-atom model. The results obtained demonstrate that polarization of the surface can be easily varied by assuming the proper charge of the model. The model in which chloride atom was introduced (pyr$-Ag_9-$Cl) produces a very poor enhancement of the bands and their improper relative intensities, comparable to the pyr$-Ag_5$ cluster. However, the pyr$-Ag_9-Cl^-$ model, in which the negative charge was set on Cl, resulted in relative intensities of the bands similar to the pyr$-Ag_{25}$ system and qualitatively comparable with the electrode SERS spectra under very negative potential.

Conclusions

The most intense bands in the fingerprint region of SERS spectra of pyridine at Ag colloids are υ_1 and υ_{12}, although their ratio depends on the applied colloid, the way in which it is activated, and the excitation wavelength. The intensity of the υ_1 band increases systematically with respect to υ_{12} with the increase of the concentration of chloride ions. Analogical changes were noticed before for SERS spectra of pyridine on silver with the increase of the negative potential of the electrode.[14,42]

Beside experimental work, an extensive quantum-chemical modeling of pyridine molecule placed on the surface of a silver metal cluster was applied in this work. At first it has been found that the molecule has a significant freedom of movement with respect to the plane of the cluster and the optimal distance between the nitrogen atom and the silver adatom is not higher than 6 Å. With the B3LYP method at the DGDZVP level, it was possible to reproduce correctly SERS spectra of pyridine, both in silver colloid and at the electrode.

The correlation of computational predictions with the experimental findings indicates that computations of SERS spectra are very sensitive to the size of a metal cluster. It was noticed that increasing of the number of silver atoms in the model resulted in significant growth of relative intensity of *all* the bands and particularly υ_{6a}, υ_1, υ_9, and υ_{8a}. This behavior is related to decrease of the optimized $N-Ag_{adatom}$ distance and increase of the charge on the pyridine nitrogen atom. Moreover, it is strictly associated with polarization of the metal surface as shown by the comparison of spectra computed for systems with 5, 9, and 25 Ag atoms (Figure 7c, d, and e) with the experimental spectra obtained from negatively polarized electrode (see Figure 6). The same effect observed also for colloidal systems due to introduction of chloride ions (Figure 5a and d) is much more subtle but can be quite properly modeled when negative charge is set on Cl in the nine-silver-atom model (Figure 7b).

Acknowledgment. Calculations were done at the Academic Computer Center "Cyfronet", Krakow, Poland (Grant KBN/SGI_ORIGIN_2000/UJ/044/1999), which is acknowledged for computing time.

Supporting Information Available: Optimized geometries of pyridine and pyridine$-Ag_{25}$; vibrational frequencies and Raman intensities of pyridine and pyridine−water complex; Raman shift of pyridine SERS spectra (Tables S1−S5); calculated Raman spectra of pyridine$-Ag_{25}$ and $(\text{pyridine}-Ag_{25})^+$ (Figure S1). This material is available free of charge via the Internet at http://pubs.acs.org.

References and Notes

(1) Fleischmann, M.; Hendra, P. J.; McQuillan, A. J. *Chem. Phys. Lett.* **1974**, *26*, 163.
(2) Albrecht, M. G.; Creighton, J. A. *J. Am. Chem. Soc.* **1977**, *99*, 5215.
(3) Jeanmaire, D. L.; Van Duyne, R. P. *J. Electroanal. Chem.* **1977**, *84*, 1.
(4) Zhao, L. L.; Jensen, L.; Schatz, G. C. *J. Am. Chem. Soc.* **2006**, *128*, 2911.
(5) Tian, Z. Q.; Ren, B.; Wu, D. Y. *J. Phys. Chem. B* **2002**, *106*, 9463.
(6) Wu, D. Y.; Liu, X. M.; Duan, S.; Xu, X.; Ren, B.; Lin, S. H.; Tian, Z. Q. *J. Phys. Chem. C* **2008**, *112*, 4195.
(7) Li, W. H.; Li, X. Y.; Yu, N. T. *Chem. Phys. Lett.* **1999**, *305*, 303.
(8) Wu, D. Y.; Ren, B.; Jiang, Y. X.; Xu, X.; Tian, Z. Q. *J. Phys. Chem. A* **2002**, *106*, 9042.
(9) Cardini, G.; Muniz-Miranda, M.; Pagliai, M.; Schettino, V. *Theor. Chem. Acc.* **2007**, *117*, 451.
(10) Muniz-Miranda, M.; Cardini, G.; Schettino, V. *Theor. Chem. Acc.* **2004**, *111*, 264.
(11) Muniz-Miranda, M.; Pagliai, M.; Cardini, G.; Schettino, V. *J. Phys. Chem. C* **2008**, *112*, 762.
(12) Pagliai, M.; Bellucci, L.; Muniz-Miranda, M.; Cardini, G.; Schettino, V. *Phys. Chem. Chem. Phys.* **2006**, *8*, 171.
(13) Muniz-Miranda, M.; Cardini, G.; Pagliai, M.; Schettino, V. *Chem. Phys. Lett.* **2007**, *436*, 179.
(14) Arenas, J. F.; Tocon, I. L.; Otero, J. C.; Marcos, J. I. *J. Phys. Chem.* **1996**, *100*, 9254.
(15) Cardini, G.; Muniz-Miranda, M.; Schettino, V. *J. Phys. Chem. B* **2004**, *108*, 17007.
(16) Johansson, P. *Phys. Chem. Chem. Phys.* **2005**, *7*, 475.
(17) Vivoni, A.; Birke, R. L.; Foucault, R.; Lombardi, J. R. *J. Phys. Chem. B* **2003**, *107*, 5547.
(18) Wu, D. Y.; Duan, S.; Ren, B.; Tian, Z. Q. *J. Raman Spectrosc.* **2005**, *36*, 533.
(19) Wu, D. Y.; Hayashi, M.; Lin, S. H.; Tian, Z. Q. *Spectrochim. Acta, Part A* **2004**, *60*, 137.
(20) Campion, A.; Ivanecky, J. E.; Child, C. M.; Foster, M. *J. Am. Chem. Soc.* **1995**, *117*, 11807.
(21) Hildebrand, P.; Stockburger, M. *J. Phys. Chem.* **1984**, 5935.
(22) Jiang, X.; Campion, A. *Chem. Phys. Lett.* **1987**, 140.
(23) Smith, W. E.; Rodger, C. Surface-Enhanced Raman Scattering. In *Handbook of Vibrational Spectroscopy*; Chalmers, J. M., Griffiths, P. R., Eds.; John Wiley & Sons, Ltd.: Chichester, U.K., 2002; Vol. 1, p 775.
(24) Jensen, L.; Zhao, L. L.; Schatz, G. C. *J. Phys. Chem. C* **2007**, *111*, 4756.
(25) Moskovits, M. *Rev. Mod. Phys.* **1985**, *57*, 783.
(26) Otto, A.; Mrozek, I.; Grabhorn, H.; Akemann, W. *J. Phys.: Condens. Matter* **1992**, *4*, 1143.
(27) Leopold, N.; Lendl, B. *J. Phys. Chem. B* **2003**, *107*, 5723.
(28) Creighton, J. A.; G., B. C.; G., A. M. *J. Chem. Soc, Faraday Trans II* **1979**, *75*, 790.
(29) Lee, P. C.; Meisel, D. *J. Phys. Chem.* **1982**, *86*, 3391.

(30) Frisch, M. J.; Trucks, G. W.; Schlegel, H. B.; Scuseria, G. E.; Robb, M. A.; Cheeseman, J. R.; Montgomery, J. A., Jr.; Vreven, T.; Kudin, K. N.; Burant, J. C.; Millam, J. M.; Iyengar, S. S.; Tomasi, J.; Barone, V.; Mennucci, B.; Cossi, M.; Scalmani, G.; Rega, N.; Petersson, G. A.; Nakatsuji, H.; Hada, M.; Ehara, M.; Toyota, K.; Fukuda, R.; Hasegawa, J.; Ishida, M.; Nakajima, T.; Honda, Y.; Kitao, O.; Nakai, H.; Klene, M.; Li, X.; Knox, J. E.; Hratchian, H. P.; Cross, J. B.; Bakken, V.; Adamo, C.; Jaramillo, J.; Gomperts, R.; Stratmann, R. E.; Yazyev, O.; Austin, A. J.; Cammi, R.; Pomelli, C.; Ochterski, J. W.; Ayala, P. Y.; Morokuma, K.; Voth, G. A.; Salvador, P.; Dannenberg, J. J.; Zakrzewski, V. G.; Dapprich, S.; Daniels, A. D.; Strain, M. C.; Farkas, O.; Malick, D. K.; Rabuck, A. D.; Raghavachari, K.; Foresman, J. B.; Ortiz, J. V.; Cui, Q.; Baboul, A. G.; Clifford, S.; Cioslowski, J.; Stefanov, B. B.; Liu, G.; Liashenko, A.; Piskorz, P.; Komaromi, I.; Martin, R. L.; Fox, D. J.; Keith, T.; Al-Laham, M. A.; Peng, C. Y.; Nanayakkara, A.; Challacombe, M.; Gill, P. M. W.; Johnson, B.; Chen, W.; Wong, M. W.; Gonzalez, C.; Pople, J. A. *GAUSSIAN 03*, revision E.01; Gaussian, Inc.: Wallingford, CT, 2004.

(31) Becke, A. D. *Phys. Rev. A* **1988**, *38*, 3098.

(32) Lee, C. T.; Yang, W. T.; Parr, R. G. *Phys. Rev. B* **1988**, *37*, 785.

(33) Sosa, C.; Andzelm, J.; Elkin, B. C.; Wimmer, E.; Dobbs, K. D.; Dixon, D. A. *J. Phys. Chem.* **1992**, *96*, 6630.

(34) Csaszar, P.; Pulay, P. *J. Mol. Struct.* **1984**, *114*, 31.

(35) Farkas, O.; Schlegel, H. B. *J. Chem. Phys.* **1999**, *111*, 10806.

(36) Barone, V.; Cossi, M. *J. Phys. Chem. A* **1998**, *102*, 1995.

(37) Cossi, M.; Rega, N.; Scalmani, G.; Barone, V. *J. Comput. Chem.* **2003**, *24*, 669.

(38) Cioslowski, J. *J. Am. Chem. Soc.* **1989**, *111*, 8333.

(39) Michalska, D.; Wysokinski, R. *Chem. Phys. Lett.* **2005**, *403*, 211.

(40) Pulay, P.; Fogarasi, G.; Pang, F.; Boggs, J. E. *J. Am. Chem. Soc.* **1979**, *101*, 2550.

(41) Martin, J. M. L.; Van Alsenoy, C. GAR2PED, University of Antwerp, 1995.

(42) Creighton, J. A. *Surf. Sci.* **1986**, *173*, 665.

(43) Sánchez-Cortés, S.; García-Ramos, J. V.; Morcillo, G.; Tinti, A. *J. Colloid Interface Sci.* **1995**, *175*, 358.

(44) Canamares, M. V.; Garcia-Ramos, J. V.; Sanchez-Cortes, S.; Castillejo, M.; Oujja, M. *J. Colloid Interface Sci.* **2008**, *326*, 103.

JP912071A